comprehension of analyses such as the 1:1 relationship, KL and DL^{-2} between human skin and cultured human skin will help clarify the characteristics of cultured skin models in skin permeation experiments.

Conclusion

Evaluation of a 1:1 relationship in P values between excised human cadaver skin and cultured skin model is crucial if we want to use a cultured human skin model as an alternative membrane for skin permeation experiments. A few cultured human skin models showed a fairly good relationship in P values compared to human skin. The difference in P and KL values in a cultured skin model compared to human skin may lead a false positive or negative in skin corrosion/irritation experiments because the chemical compound concentration in skin is determined by the parameterd (Sugibayashi *et al.*, 2009). The reason for the difference in P values compared to excised human skin remains unclear, so further experiments will need to clarify not only skin permeation experiments, but also total extracellular lipid constitution determined by X-ray small angle scattering analysis (Ponec *et al.*, 2000; Hatta *et al.*, 2001) and transmission electron microscopy observation.

Acknowledgement

A part of this research was supported by the first Mandom International Research Grants on Alternative to Animal Experiments.

References

Asbill C., Kim N., El-Kattan A., Creek K., Wertz P., and Michniak B. (2000) Evaluation of a human bio-engineered skin equivalent for drug permeation studies, *Pharm. Res.*, 17, 1092-1097.

Desai S.J., Simonelli A.P. and Higuchi W.I. (1965) Investigation of factors influencing release of solid drug dispersed in inert matrices, *J. Pharm. Sci.*, 54, 1459-1464.

Downing D.T., Wertz P.W., and Stewart M.E. (1986) The role of sebum and epidermal lipids in the cosmetic properties of skin, *Int. J. Cosmet. Sci.*, 8,115-123.

Gabbanini S., Lucchi E., Carli M., Berlini E., Minghetti A., and Valgimigli L. (2009) In vitro evaluation of the permeation through reconstructed human epidermis of essentials oils from cosmetic formulations, *J. Pharm. Biomed. Anal.*,50, 370-376.

Hammell D.C., Stolarczyk E.I., Klausner M., Hamad M.O., Crooks P.A., and Stinchcomb A.L. (2005) Bioconversion of naltrexone and its 3-*o*-alkyl-ester prodrugs in a human skin equivalent, *J. Pharm. Sci.*, 94, 828-836.

Hatta I., Ohta N., Ban S., Tanaka H., and Nakata S. (2001) X-ray diffraction study on ordered, disordered and reconstituted intercellular lipid lamellar structure in stratum corneum. *Biophys. Chem.*, 89, 239-242.

Kano S., and Sugibayashi K. (2006) Kinetic analysis on the skin disposition of cytotoxicity as an index of skin irritation produced by cetylpyridinium chloride:comparison *in vitro* data using a three-dimensional cultured human skin model with *in vivo* results in hairless mice, *Pharm Res*, 23, 329-335.

Lotte C., Patouillet C., Zanini M., Messager A., and Roguet R. (2002) Permeation and skin absorption: Reproducibility of various industrial reconstructed human skin models, *Skin Pharmacol. Appl. Skin Physiol.*,15, 18-30.

Morimoto Y., Hatanaka T., Sugibayashi K. and Omiya H. (1992) Prediction of skin permeability of drugs: comparison of human and hairless rat skin, *J. Pharm. Pharmacol.*,44, 634-639.

Netzlaff F., Kaca M., Bock U., Haltner-Ukomadu E., Meiers P., Lehr C.M. and Schaefer U.F. (2007) Permeability of the reconstructed human epidermis model Episkin in comparison to various human skin preparations, *Eur. J. Pharm. Biopharm.*, 66, 127-134.

Ponec M., Boelsma E., Weerheim A., Mulder A., Bouwstra J. and Mommaas M. (2000) Lipid and ultrastructural characterization of reconstructed skin models, *Int. J. Pharm.*, 203, 211-225.

Ponec M., Boelsma E., Gibbs S. and Mommaas M. (2002) Characterization of reconstructed skin models, *Skin Pharmacol. Appl. Skin Physiol.*, 15, 4-17.

Scheuplein R.J. (1967) Mechanism of percutaneous absorption II. Transient diffusion and the relative importance of various routes of skin penetration, *J. Invest. Dermatol.*, 48, 79-88.

Schmook F.P, Meingassner J.G., and Billich A. (2001) Comparison of human skin or epidermis models with human and animal skin in in-vitro percutaneous absorption, *Int.J. Pharm.*, 215, 51-56.

Shah J. C. (1993) Analysis of permeation data: evaluation of the lag time method, *Int. J.Pharm.*, 90, 161-169.

Sugibayashi K., Watanabe T., Hasegawa T., Takahashi H. and Ishibashi T. (2002) Kinetic analysis on the in vitro cytotoxicity using Living Skin Equivalent for ranking the toxic potential of dermal irritants, *Toxicol. In Vitro*, 16 759-763.

Sugibayashi K., Hayashi T., Matsumoto K., and Hasegawa T. (2004) Utility of a three-dimensional cultured human skin model as a tool to evaluate the simultaneous diffusion and metabolism of ethyl nicotinate in skin, *Drug Metab. Pharmacokinet.*, 19, 352-362.

Sugibayashi K., Todo H., Oshizaka T. and Owada Y. (2010) Mathematical model to predict skin concentration of drugs: toward utilization of silicone membrane to predict skin concentration of drugs as an animal testing alternative, *Pharm. Res.*, 27, 134-142.

Young D.F. and Ball W.P. (1965) Estimating diffusion coefficients in low-permeability porous media using a macropore column, *Environ. Sci. Technol.*, 32, 2578-2584.

Wagner H., Kostka K.H., Lehr C.M., and Schaefer U.F. (2001) Interrelation of permeation and penetration parameters obtained from in vitro experiments with human skin and skin equivalents, *J. Control. Release,* 75, 283-295.

Watanabe T., Hasegawa T., Takahashi H., Ishibashi T., Takayama K. and Sugibayashi K. (2001) Utility of the three-dimensional cultured human skin model as a tool to evaluate skin permeation of drugs, *Altern. Animal Test EXperiment*, 8, 1-14.

Watanabe T., Hasegawa T., Takahashi H., Ishibashi T., Itagaki H. and Sugibayashi K.(2002) Utility of MTT assay in three-dimensional cultured human skin model as an alternative for draze skin irritation test: approach using diffusion law of irritation in skin and toxicokinetics-toxicodynamics correlation, *Pharm. Res.*, 19, 669-675.

Williams M.L., and Elias P.M. (1987) The extracellular matrix of stratum corneum: Role of lipids in normal and pathological function, *Crit. Rev. Ther. Drug Carrier Syst.*, 3, 95-122.

(Received: July 25 /
Accepted: October 18)

Corresponding author:
Kenji Sugibayashi, Ph.D
Faculty of Pharmaceutical Sciences,
Josai University
1-1 Keyakidai, Sakado,
Saitama 350-0295, Japan
E-mail: sugib@josai.ac.jp

Permeation Pathway of Macromolecules and Nanospheres through Skin

Hiroaki Todo,[a] Eriko Kimura,[a] Hirotaka Yasuno,[a] Yoshihiro Tokudome,[a] Fumie Hashimoto,[a] Yoshiaki Ikarashi,[b] and Kenji Sugibayashi*,[a,c]

[a] *Faculty of Pharmaceutical Sciences, Josai University;* [c] *Life Science Research Centre, Josai University; 1–1 Keyakidai, Sakado, Saitama 350–0295, Japan: and* [b] *National Institute of Health Sciences; 1–18–1 Kamiyoga, Setagaya-ku, Tokyo 158–8501, Japan.* Received February 15, 2010; accepted May 31, 2010; published online June 1, 2010

The permeation pathway of macromolecules and nanospheres through skin was evaluated using fluorescent isothiocyanate (FITC)-dextran (average MW, 4 kDa) (FD-4) and nanospheres (500 nm in diameter) in hairless rat abdominal skin and porcine ear skin as well as a three-dimensional cultured human skin model (cultured skin model). A low molecular hydrophilic compound, sodium fluorescein (FL) (MW, 376 Da), was used for comparison. FL penetrated the stratum corneum and permeated the viable epidermis of hairless rat skin, whereas less permeation of FL was observed through the cultured skin model, suggesting that the primary permeation pathway for the hydrophilic material may be skin appendages through the rat skin. A macromolecular compound, FD-4, was distributed through the hair follicles of the rat skin. In addition, nanospheres were detected in the hair follicles of porcine skin, although no skin permeation was detected. These findings suggest that appendage routes such as hair follicles can be a penetration pathway of macromolecules and nanospheres through skin.

Key words macromolecule; nanosphere; skin permeation pathway; transdermal drug delivery; hair follicle

Delivery of macromolecular compounds and nano-/microparticles has become more realistic due to the recent development of new tools and nanotechnologies for delivery enhancement.[1,2] The administration sites of such macromolecules and nano-/microparticles are supposed to be the mucosa, such as the gastrointestinal (GI) tract,[3] and ophthalmic, nasal and pulmonary[4] mucosa and skin.[5,6] Skin has been paid particular attention as an attractive administration site of these compounds because of its accessibility and easy application. Emulsion droplets, liposomes and other lipophilic carriers[7] containing small molecular active ingredients have already been investigated in the cosmetic field as well as therapeutic drug areas; however, the stratum corneum, the outermost layer of skin, has a primary function to protect the invasion and skin penetration of exogenous substances. Generally, only small molecular compounds less than 500 Da molecular weight are capable of significant passive permeation through the skin barrier (known as the 500 Dalton rule).[8] Thus, skin permeation of macromolecular compounds or nano-/microparticles is very difficult or impossible. Many reports have suggested that large molecules are likely to accumulate on the skin surface or appendages such as hair follicles.[9—12] Nevertheless, few reports have shown a quantitative approach for hair follicular penetration using quantitative skin permeation parameters.

Hairless rat and pig ear skins and three-dimensional cultured human skin model would be useful skin models with and without hair follicles, respectively, to clarify the contribution of hair follicles to skin permeation or the distribution of macromolecules and nanospheres.

In the present study, we selected fluorescent isothiocyanate (FITC)-dextran (average MW, 4 kDa) (FD-4) as a model macromolecular weight compound and 500 nm fluorescent polystyrene latex spheres as model nanospheres, and their potential for skin delivery was investigated by calculating skin permeation parameters or measuring the skin distribution of FD-4 and fluorescent polystyrene latex nanospheres in hairless rat abdominal skin and porcine ear skin as well as a three-dimensional cultured human skin model. Tables 1 and 2 summarize the model penetrant compounds and skin membranes used in this experiment. A low molecular hydrophilic compound, sodium fluorescein (FL) (MW 376 Da), was also used for comparison.

Theoretical Skin permeation kinetics is usually evaluated under an assumption that the skin consists of a single barrier membrane against drug permeation; however, generally, the drug-permeable membrane must be classed into three membranes: dissolution–diffusion membrane (Type 1 membrane), porous membrane (Type 2 membrane) and composite membrane (Type 3 membrane) of Type 1 and 2 membranes. Under the assumption that a single barrier of skin is one of these three membranes, the steady state skin permeation rate per unit application area, dQ/dt, is expressed using Fick's first law of diffusion as follows:

Type 1 membrane (dissolution–diffusion membrane)

$$\frac{dQ}{dt} = D \cdot \frac{K \cdot C_v}{L} = (KL)\left(\frac{D}{L^2}\right)C_v \tag{1}$$

Type 2 membrane (porous membrane)

$$\frac{dQ}{dt} = \frac{\varepsilon \cdot D_p}{\tau} \cdot \frac{C_v}{L} = (\varepsilon L)\left(\frac{D_p}{\tau L^2}\right)C_v \tag{2}$$

Type 3 membrane (composite membrane)

$$\frac{dQ}{dt} = (1-\varepsilon) \cdot D \cdot \frac{K \cdot C_v}{L} + \frac{\varepsilon \cdot D_p}{\tau} \cdot \frac{C_v}{L} = \left[\{(1-\varepsilon)KL\}\left(\frac{D}{L^2}\right) + (\varepsilon L)\left(\frac{D_p}{\tau L^2}\right)\right]C_v \tag{3}$$

where C_v is the initial concentration of the applied compound, D, K and L are diffusion coefficient, partition coefficient and barrier thickness of the membrane, respectively, and D_p, ε and τ are diffusion coefficients in water-filled pores, average fraction of diffusion area of pores, and tortuosity of the membrane, respectively. In examples 1 and 2, partition parameters and diffusion parameters of the pene-

* To whom correspondence should be addressed. e-mail: sugib@josai.ac.jp

trant are KL and DL^{-2} for the Type 1 membrane and εL and $D_p\tau^{-1}L^{-2}$ for the Type 2 membrane, respectively. The permeability coefficient, P, can be obtained as a product of the partition parameter and diffusion parameter. Diffusion lag time was obtained by dividing six by the diffusion parameter.

MATERIALS AND METHODS

Materials and Animals Both FL and FD-4 were obtained from Sigma-Aldrich Co., Ltd. (St. Louis, MO, U.S.A.). Fluorescent polystyrene latex nanospheres, Fluoresbrite® yellow green carboxylate microspheres (500 nm in average diameter), were purchased as model nanospheres from Polysciences, Inc. (Warrington, PA, U.S.A.). All other reagents and solvents were of reagent grade or HPLC grade, and used without further purification.

Male hairless rats (WBN/ILA-Ht, *ca.* 200—250 g) were supplied either from Life Science Research Center, Josai University (Sakado, Saitama, Japan) or Ishikawa Experimental Animal Laboratory (Fukaya, Saitama, Japan). Porcine ear skins were from Saitama Experimental Animal Laboratory (Sugito, Saitama, Japan). A three-dimensional cultured human skin model, Living Skin Equivalent-high (LSE-high), was obtained from Toyobo (Osaka, Japan).

Determination of *n*-Octanol–Water Partition Coefficient *n*-Octanol–water partition coefficient ($K_{o/w}$) of each fluorescent compound (FL or FD-4) was measured using distilled water–saturated *n*-octanol and *n*-octanol–saturated pH 7.4 phosphate buffered saline (PBS) at 32 °C. *n*-Octanol was added to the same volume of pH 7.4 PBS containing 10 mg/ml of each fluorescent, and the thoroughly mixed solution was equilibrated for 24 h. The aqueous phase was then analyzed using a fluorescence spectrophotometer (RF 5300PC; Shimadzu, Kyoto, Japan) at excitation and emission wavelengths of 490 and 520 nm, respectively. Logarithmic values of the partition coefficients are shown in Table 1.

***In Vitro* Skin Permeation Study** The skin permeation of FL and FD-4 was assessed using excised hairless rat abdominal skin and LSE-high. After the rats had been anesthetized by intraperitoneal injection of sodium pentobarbital (50 mg/kg), the abdominal skin was excised as described in our previous paper.[14] Stripped hairless rat skin was also used after removing the stratum corneum from the abdominal area by stripping 20 times with adhesive tape (Cellophane tape; Nichiban Co., Ltd., Tokyo, Japan). LSE-high was used after removing cultured skin pieces from the plastic insert with a knife. Each skin membrane was mounted in the side-by-side diffusion cell (effective diffusion area: 0.95 cm^2),[15,16] and 1.0 mM FL or 0.25 mM FD-4 (2.5 ml each) was applied to the stratum corneum side and the same volume of PBS was applied to the dermal side. Samples of 0.40 ml were taken periodically from the dermal side compartment, and then the same volume of the same solvent was added to keep the volume constant. FL or FD-4 concentration of each sample was determined using a fluorescence spectrophotometer, as explained above. The hairless rat skin and LSE-high surfaces were carefully rinsed with PBS several times to remove FL or FD-4 attached to the stratum corneum 6 h after starting the experiment. The obtained skin sample was embedded in Tissue-Tek® OTC compound (Miles, Inc., Elkhart, IN, U.S.A.) and stored at −80 °C until slicing.

Table 1. Physicochemical Properties of Model Compounds

Model compounds (abbreviation)	Molecular weight (Da)	Mean particle size or molecular radius	Log $K_{o/w}$ [a]
Sodium fluorescein (FL)	376	0.45 nm[13] (Stokes radius)	−0.615
FITC-dextran (FD-4)	4000	1.4 nm (Stokes radius)[13]	−0.773
Fluorescent polystyrene latex nanospheres (Fluoresbrite)	—	500 nm	—

a) $K_{o/w}$: *n*-octanol–water partition coefficient.

The skin permeation property of fluorescent polystyrene latex spheres (Fluoresbrite) was evaluated using excised hairless rat skin and excised porcine ear skin, which had been carefully shaved and the underlying excess fatty tissues removed from the dermis. LSE-high was also used to evaluate whether Fluoresbrite permeates the cultured skin. The obtained skin membranes were mounted in a Franz-type diffusion cell[14] (effective diffusion area: 1.77 cm^2). Then, 1.0 ml PBS-suspended solution containing Fluoresbrite (3.64×10^{10} particles/ml for 500 nm spheres) was applied to the stratum corneum surface, whereas 6.0 ml PBS was applied to the dermal side. The skin permeation test was performed at 32 °C over 12 h through hairless rat skin, porcine ear skin and LSE-high, while the receiver solution was continuously stirred with a star-head-type magnetic stirrer. The receiver solution was withdrawn 12 h after beginning the permeation experiment. The skins were then carefully rinsed with PBS several times to remove polystyrene spheres attached to the stratum corneum 12 h after starting the experiment. The obtained skin sample was embedded in Tissue-Tek® OTC compound (Miles, Inc., Elkhart, IN, U.S.A.) and stored at −80 °C until slicing.

All animal experiments were approved by the Institutional Animal Care and Use Committee of Josai University.

Evaluation of Skin Permeation Kinetics Steady-state flux was calculated by linear regression of the linear portion of normalized cumulative amount of penetrant permeated *versus* the time-curve (steady state; reached 4—6 h after starting the experiment), and the lag time was calculated from the intercept on the time axis by extrapolation from the steady state skin permeation profile. The normalized cumulative amount of penetrant permeated, Q_n, was calculated by dividing the cumulative amount permeated per unit area of skin by the initial concentration of the applied fluorescent compound in the donor compartment.[17] The permeation parameters were obtained by curve fitting the skin permeation data by Scheuplein's equation,[18] which comes from Fick's second law of diffusion. The least squares curve fitting method was performed using Microsoft® Excel Solver.[19] The calculation condition was 100 s for the calculation limit, 100 times for repeated calculation, 10^{-6} for accuracy, 5% basic tolerance and 10^{-3} for convergence. The pseudo-Newtonian method was used as an algorithm.

Sectioning of Hairless Rat Skin, Porcine Ear Skin and LSE-High Hairless rat skin, porcine ear skin and LSE-high embedded in Tissue-Tek® OTC compound were sequentially sliced with a cryostat (CM3050S; Leica, Wetzlar, Germany) to obtain horizontal and vertical 20 μm-thick sections. The prepared skin sections were observed with a fluorescence mi-

Table 2. Comparison of Skin Thickness and Presence or Absence of Hair Follicles in Several Skin Models

Skin model	Skin structure constitution	Stratum corneum thickness (μm)	Epidermis thickness (μm)	Whole skin thickness (mm)	Skin appendage	Relationship to human skin permeation
Hairless rat skin	Epidermis/dermis	15.4±3.3[20]	23.8±5.3[20]	0.86±0.06[20]	Yes	High
Pig skin	Epidermis/dermis	10.6±0.5	52.5±4.1	1.2±0.002	Yes	High
LSE-high	Epidermis/dermis	27.0±0.7	31.4±1.3	0.12±0.001	No	High

croscope (CK40; Olympus Corp., Tokyo, Japan).

Measurement of Thickness in LSE-High and Porcine Skin The thicknesses of the stratum corneum, epidermis, and whole skin in LSE-high and porcine skin were microscopically determined from microtomed sections after hematoxylin–eosin staining. Five good sections from each specimen were used to measure the stratum corneum, and whole skin thicknesses were measured by a light micrograph (IX71; Olympus Corp., Tokyo, Japan) and a calibrated ocular micrometer. The thickness of the epidermis was calculated by subtracting the stratum corneum thickness from the whole skin thickness. The thickness of hairless rat skin was cited from our previous paper.[20]

Observation of Skin Surface Shaved hairless rat and porcine ear skins were mounted with adhesive tape on a scanning microscopy (SEM) stage, and the skin surface was observed without coating by a low-vacuum SEM (S-3000N; Hitachi Ltd., Tokyo, Japan).

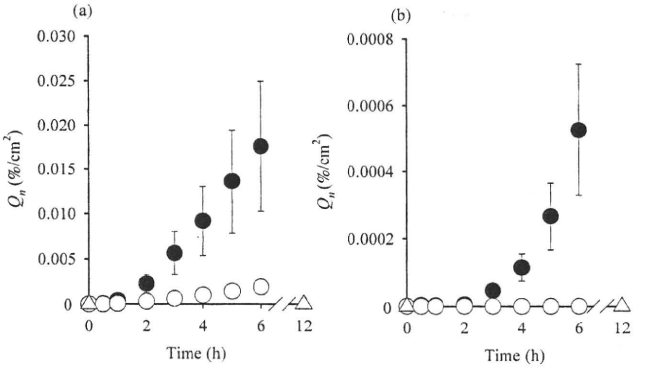

Fig. 1. Cumulative Amount of Hydrophilic Fluorescent Compounds, FL (●), FD-4 (○) and 500 nm Fluoresbrite (△) through Hairless Rat Skin (a) and LSE-High (b)

Normalized cumulative amount of the compounds permeating a percent per unit application area (%/cm^2)[17] was plotted on the vertical axis. Each data point represents the mean±S.E. of 3—4 experiments.

RESULTS

Many reports have shown that nano-/microspheres could not permeate the healthy stratum corneum.[21] In our study, therefore, the penetration pathway of hydrophilic fluorescent markers, FL and FD-4, was observed to evaluate the potential penetration of these mal-absorptive materials into skin and the delivery pathway through the skin barrier. The characteristics of model skin membranes (excised hairless rat skin, pig ear skin and LSE-high) are shown in Table 2. The stratum corneum in LSE-high was much thicker than the others. In addition, skin appendages such as sweat ducts and hair follicles could not be observed in LSE-high. Although many structural differences could be found between LSE-high and the others, and the permeation of several compounds (MW 122—236, $-1.5<\log K_{o/w}<2.1$) through LSE-high was about 10 times higher than through hairless rat and human skins, and the permeation rate through LSE-high showed a linear relationship to that through hairless rat and human skins.[14]

Figure 1a and b show the time course of the normalized cumulative amount of FL and FD-4 that permeated the unit area of excised hairless rat skin and LSE-high, respectively. In these experiments, 1.0 mM FL or 0.25 mM FD-4 (2.5 ml each) was applied to the skin surface to follow skin permeation. Interestingly, both fluorescent markers permeated hairless rat skin, whereas less permeation of FL and no permeation of FD-4 were observed through LSE-high. The Q_n of FL through hairless rat skin was 30-fold higher than through LSE-high.

The typical lag time and subsequent steady state permeation were observed for the permeation of both fluorescents through hairless rat skin. Permeability coefficients of FL and FD-4 were calculated by two methods using steady-state flux (observed value) and the curve fitting method (estimated value). These values are summarized in Table 3. The estimated vales were almost equal to the corresponding observed values and no significant differences appeared in hairless rat data. The calculated values of the permeability coefficient and Q_n of FL through LSE-high were about one-twelfth and one-thirtieth through hairless rat skin, respectively; furthermore, the lag time of FL through LSE-high (estimated value) was about three-fold of that through hairless rat skin. On the other hand, lag times of FL and FD-4 through hairless rat skin were almost the same as those through LSE-high.

Fluoresbrite was also applied to hairless rat skin and LSE-high. Although a Franz-type diffusion cell was used for measuring the skin permeation of Fluoresbrite, no permeation of the nanospheres was detected 12 h after starting the skin permeation experiment (see Fig. 1). No skin permeation was detected when Fluoresbrite was applied to porcine ear skin (data not shown).

Figure 2 shows fluorescent photographs illustrating the skin distribution of FL and FD-4 in hairless rat skin and LSE-high after topical application of these fluorescent markers. High-intensity FL was detected both in the stratum corneum and hair follicles of hairless rat (Fig. 2a), whereas FD-4 was mainly observed in the hair follicles (Fig. 2b). On the other hand, with LSE-high, FL was detected mostly in the stratum corneum and slightly in the viable epidermis (Fig. 2c) and FD-4 was found only on the skin surface (no skin penetration was observed for FD-4) (Fig. 2d). These results also suggest the high contribution of the transfollicular pathway to the transport of mal-absorptive hydrophilic compounds across the skin. In addition, this tendency was more

Table 3. Lag Time and Permeability Coefficients of FL and FD-4 through Excised Hairless Rat Skin or LSE-High

		FL		FD-4	
		Lag time (h)	Permeability coefficient (cm/s)	Lag time (h)	Permeability coefficient (cm/s)
Hairless rat	Estimated value[a)]	2.0±0.16	$(1.1\pm0.5)\times10^{-8}$	2.2±0.01	$(3.6\pm0.2)\times10^{-9}$
	Observed value[b)]	1.8±0.20	$(1.2\pm0.5)\times10^{-8}$	2.1±0.01	$(3.4\pm0.2)\times10^{-9}$
LSE-high	Estimated value[a)]	5.4±0.4	$(9.4\pm2.4)\times10^{-10}$	—	$\ll1.21\times10^{-10}$ [d)]
	Observed value[b)]	—[c)]	—[c)]	—[c)]	—[c)]

a) Estimated value was calculated by curve-fitting the time course of the cumulative amount of skin permeation of compounds using Scheuplein's equation.[25] *b*) Observed value was obtained by the slope of steady-state flux and time–axis intercept of the time course of the cumulative amount of skin permeation of compounds. *c*) No steady state permeation was obtained until 6 h in the skin permeation study. *d*) Estimated value was calculated from lower quantitative limit of FD-4 in receiver cell 6 h after skin permeation study.

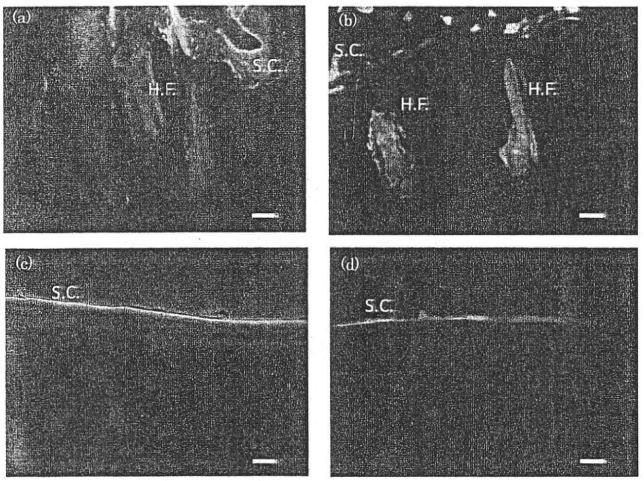

Fig. 2. Histological Observation of Hairless Rat Intact Skin (a, b) and LSE-High (c, d) after Application of FL (a, c) and FD-4 (b, d)

S.C.: Stratum corneum; H.F.: hair follicle. White bars=100 μm. (a, b): Fluorescence derived from FL or FD-4 was observed on the skin surface of skin and in hair follicles, (c, d): fluorescence derived from FL or FD-4 was observed in shallow areas or only on the surface, respectively, of LSE-high.

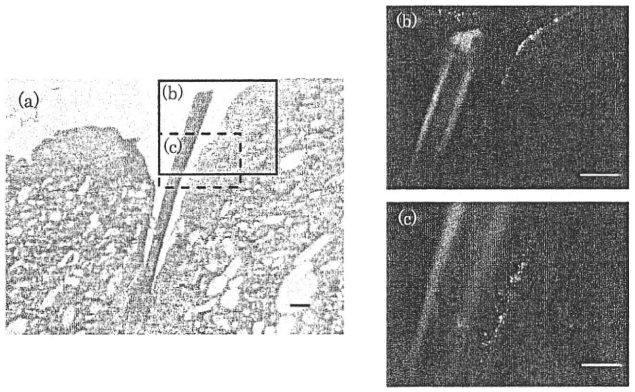

Fig. 3. Histological Observation of Excised Porcine Ear Skin 12 h after Application of 500 nm Fluoresbrite

a: Light micrograph of vertical slice. b and c: Fluorescent micrograph of area b and c in Fig. 3a. Bar=200 μm. (b, c): Fluoresbrite was observed in infundibulum of the hair follicle and surface of the hair shaft.

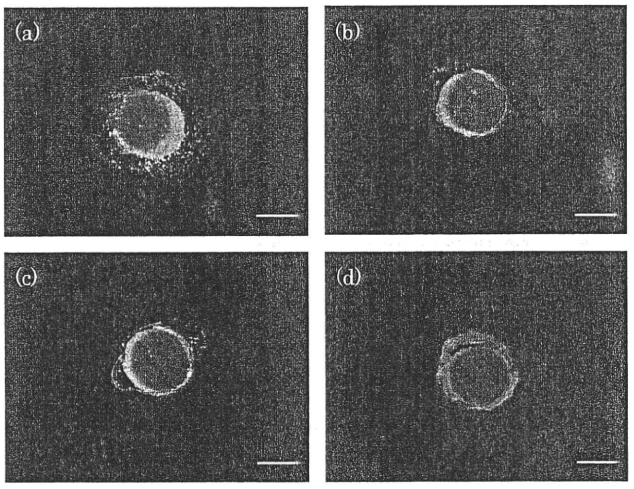

Fig. 4. Localization of 500 nm Fluoresbrite Penetrating the Hair Follicle

Fluorescence images (a—d) are horizontal slices at different depths from the skin surface of excised porcine ear skin 12 h after application of particles. a: *ca.* 20 μm, b: 40—60 μm, c: 80—100 μm, d: 200—220 μm. Bar=100 μm. (a): Fluoresbrite was detected on the surface of hair shaft and connective tissue in the follicle, (b, c): number of particles gradually decreased with an increase in depth from the skin surface, (d) only autofluorescence was observed.

marked when using the macromolecular compound. Thus, skin appendages such as hair follicles must be very important for the skin permeation of malabsorptive compounds.

Next, the skin distribution of Fluoresbrite (500 nm in diameter) was investigated after topical application to excised hairless rat skin, excised porcine ear skin and LSE-high. Nanospheres were detected only on the surface of the stratum corneum (data not shown) for hairless rat skin and LSE-high; therefore, a detailed observation was performed using excised porcine skin, since it has much larger hair follicles. Figure 3a shows a light microphotograph of porcine skin (vertical slice of hair follicle area) 12 h after the application of Fluoresbrite, and Figure 3b and c show fluorescent microphotographs of specific parts of the hair follicle area, as explained in Fig. 3a. Many nanospheres were found around the openings of the hair follicle, especially close to the epidermis side and around the hair shaft, as shown in Fig. 3b and c. The penetration depth of Fluoresbrite in the hair follicles was investigated by preparing horizontal slices of the hair follicle area of skin. The thickness of each skin section was adjusted to 20 μm. Figure 4 shows typical cross-section images of the hair follicle area from the skin surface (0—20 μm) to dermis side (200—220 μm) 12 h after application of Fluoresbrite to the excised porcine ear skin. In accordance with the photograph in Fig. 3, nanospheres could be detected in hair follicles, such as the surface of the hair shaft and connective tissue follicles, and the intensity due to nanospheres in the hair follicle gradually decreased with increasing pene-

tration depth; however, nanospheres could not be detected in connective tissue follicles below 200-μm depth from the skin surface. Only greenish-yellow autofluorescence derived from keratin and melanin was observed in Fig. 4d. This result clearly identified that the nanospheres were distributed or penetrated until about 100-μm depth, but did not penetrate as far as 200-μm depth from the skin surface 12 h after application. Thus, macromolecular compounds, such as FD-4 and nanospheres, are probably distributed or penetrate through the transfollicular pathway, although the extent is very marginal.

DISCUSSION

Three kinds of membranes are frequently utilized to describe the membrane permeation profiles of compounds, as explained in the theoretical section. In the dissolution–diffusion membrane (Type 1 membrane), compounds are dissolved and distributed into the membrane and then diffused in the homogeneous membrane. In the microporous membrane (Type 2 membrane), compounds are diffused across solvent (usually aqueous)-filled pores in the membrane. The third membrane (composite membrane) is the previous two membranes combined.

In the case of hairless rat and porcine skins, the stratum corneum and skin appendage may be the permeation pathway of compounds, especially for low molecular compounds ($\leq$500 Da). Thus, these animal skins would be assumed to be the third membrane. On the other hand, LSE-high would be classified as a dissolution–diffusion membrane, since three-dimensional cultured human skin model has no appendages, such as hair follicles and sweat ducts.

Although LSE-high is such a skin appendage-deficiency model, it was observed in our previous study[14] that logarithmic values of the permeability coefficient, log P, of seven drugs through LSE-high were fairly proportional to those through excised hairless rat, pig and human skins, and the partition parameters of LSE-high were almost the same as in other skins. For FL and FD-4 applied to LSE-high, low permeation and no permeation were observed in the present study, while permeation through hairless rat skin was observed. The permeability coefficient, P, of FD-4 through LSE-high was calculated from the lower quantitative limit of FD-4 in receiver solution (Table 3). The estimated value was about thirtieth of that of FD-4 through hairless rats. FL (pK_a 1: 4.32, pK_a 2: 6.5)[22] predominantly exists as an ionized form in pH 7.4 PBS, and FD-4 has a high molecular weight; therefore, the P-value of FL and FD-4 through LSE-high was much lower than through hairless rat skin.

The P-value is a product of the partition parameter (KL or εL) and diffusion parameter (DL^{-2} or $D_p\tau^{-1}L^{-2}$).[23] To clarify the differences of skin permeation profiles between hairless rat skin and LSE-high, the partition parameter and diffusion parameter were compared.

Table 4 shows the partition and diffusion parameters, which were calculated from curve-fitting the time course of the cumulative amount of FL and FD-4 permeating hairless rat skin and LSE-high. Interestingly, both parameters of LSE-high calculated from FL permeation were not the same as those of hairless rat skin. These differences might reflect the different permeation routes of FL between these skins.

Table 4. Comparison of Partition Parameter and Diffusion Parameter between Hairless Rat Skin and LSE-High

Compound	Membrane	Partition parameter (KL or εL) (cm)	Diffusion parameter (DL^{-2} or $D_p\tau^{-1}L^{-2}$) (s^{-1})
FL	Hairless rat	$(4.7\pm1.8)\times10^{-4}$	$(2.3\pm0.18)\times10^{-5}$
	LSE-high	$(1.1\pm0.31)\times10^{-4}$	$(8.6\pm0.75)\times10^{-6}$
FD-4	Hairless rat	$(1.7\pm0.13)\times10^{-4}$	$(2.0\pm0.06)\times10^{-5}$
	LSE-high	—	—

KL and DL^{-2} or εL and $D_p\tau^{-1}L^{-2}$ were calculated by curve-fitting the skin permeation profile of FL and FD-4 through hairless rat skin and LSE-high.

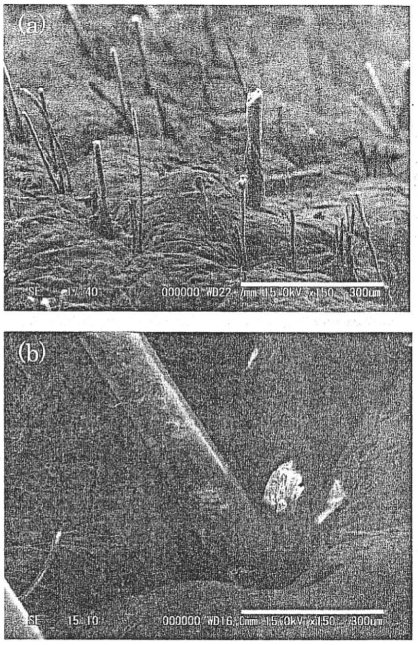

Fig. 5. SEM Observation of Hairless Rat Skin (a) and Porcine Ear Skin (b)

Bar=300 μm.

Increased partition and diffusion parameters of FL in hairless rat skin might mean that FL was mainly partitioned in pore routes and permeated the pore routes of skin; therefore, skin appendages, such as hair follicles, are the predominant permeation route of FL.

The diffusion parameters of FL and FD-4 in hairless rat skin showed almost the same value due to the slight difference in the cubic root of the molecular weight of these compounds, because the diffusion coefficient is proportional to the reciprocal of the cubic root, which is given by the Stokes–Einstein equation. Therefore, FL and FD-4 must permeate through almost the same permeation pathway of skin. On the other hand, the partition parameter of FD-4 was about one-third that of FL, indicating that FD-4 permeated skin through a more restricted pathway, such as hair follicles, than the FL pathway. In addition to this assumption, the present fluorescence images strongly supported the skin appendage route as a useful pathway for skin permeation and/or the distribution of such macromolecular compounds.

Fluoresbrite did not permeate hairless rat skin or LSE-high. Thus, porcine skin was selected to observe its skin distribution because the pores of hair follicles in porcine skin

are larger than in hairless rat skin (see Fig. 5). Fluoresbrite was especially observed in the infundibulum of hair follicles of porcine skin and no spheres were observed more than 100-μm depth from the skin surface (Fig. 4). It is reasonable that Fluoresbrite was detected only in the hair follicle because even FD-4, having a smaller molecular radius than nanospheres, was mainly detected in hair follicles.

This indicated that hair follicles are expected to be a useful pathway, not only for macromolecular compounds, but also nanospheres, through the skin barrier. Scheuplein[18] reported that the contribution of the transappendage route to the skin permeation of low molecular compounds must be very low, although the transfollicular pathway would play a very important role in the early stage of skin permeation and distribution. This is because the skin appendage area is only 0.1% of the total skin surface area.[18,24] Further study is necessary to fully elucidate the contribution of hair follicles to the skin permeation or distribution of hydrophilic compounds and nano-/microspheres. This contribution of hair follicles can be assessed using skin permeation parameters, such as $\varepsilon \cdot L$ and $D/\tau \cdot L^2$ as above.

CONCLUSION

The present study revealed that important role of hair follicles as a permeation pathway or distribution pathway for hydrophilic compounds and nanospheres. Although not only skin features, such as hair density and follicle size, but also physicochemical properties, such as molecular size and *n*-octanol/water partition coefficient of compounds, affect their transfollicular permeation,[25] analysis of the hair follicle contribution to the overall skin permeation of compounds using permeation parameters will help to understand efficient compound targeting of hair follicles.

Acknowledgement This study was supported by a Grant-in-Aid for Scientific Research (H20-iyaku-ippan-001) from the Ministry of Health, Labor, and Welfare, Japan.

REFERENCES

1) Ravi Kumar M. N., *J. Pharm. Pharm. Sci.*, **3**, 234—258 (2000).
2) Bilati U., Allemann E., Doelker E., *Eur. J. Pharm. Biopharm.*, **59**, 375—388 (2005).
3) Takeuchi H., Matsui Y., Sugihara H., Yamamoto H., Kawashima Y., *Int. J. Pharm.*, **303**, 160—170 (2005).
4) Todo H., Iida K., Okamoto H., Danjo K., *J. Pharm. Sci.*, **92**, 2475—2486 (2003).
5) Alvarez-Roman R., Naik A., Kalia Y. N., Guy R. H., Fessi H., *J. Controlled Release*, **99**, 53—62 (2004).
6) Almeida A. J., Souto E., *Adv. Drug Deliv. Rev.*, **59**, 478—490 (2007).
7) Honeywell-Nguyen P. L., Wouter Groenink H. W., Bouwstra J. A., *J. Liposome Res.*, **16**, 273—280 (2006).
8) Bos J. D., Meinardi M. M., *Exp. Dermatol.*, **9**, 165—169 (2000).
9) Lademann J., Weigmann H., Rickmeyer C., Barthelmes H., Schaefer H., Mueller G., Sterry W., *Skin Pharmacol. Appl. Skin Physiol.*, **12**, 247—256 (1999).
10) Toll R., Jacobi U., Richter H., Lademann J., Schaefer H., Blume-Peytavi U., *J. Invest. Dermatol.*, **123**, 168—176 (2004).
11) Trauer S., Patzelt A., Otberg N., Knorr F., Rozycki C., Balizs G., Buttemeyer R., Linscheid M., Liebsch M., Lademann J., *Br. J. Clin. Pharmacol.*, **68**, 181—186 (2009).
12) Teichmann A., Jacobi U., Ossadnik M., Richter H., Koch S., Sterry W., Lademann J., *J. Invest. Dermatol.*, **125**, 264—269 (2005).
13) Mota M. C., Carvalho P., Ramalho J., Leite E., *Int. Ophthalmol.*, **15**, 321—326 (1991).
14) Watanabe T., Hasegawa T., Takahashi H., Ishibashi T., Takayama K., Sugibayashi K., *Altern. Animal Test Experiment.*, **8**, 1—14 (2001).
15) Okumura M., Sugibayashi K., Ogawa K., Morimoto Y., *Chem. Pharm. Bull.*, **37**, 1404—1406 (1989).
16) Obata Y., Takayama K., Maitani Y., Machida Y., Nagai T., *Biol. Pharm. Bull.*, **16**, 312—314 (1993).
17) Sugibayashi K., Hosoya K., Morimoto Y., Higuchi W. I., *J. Pharm. Pharmacol.*, **37**, 578—580 (1985).
18) Scheuplein R. J., *J. Invest. Dermatol.*, **48**, 79—88 (1967).
19) Sugibayashi K., Hayashi T., Matsumoto K., Hasegawa T., *Drug Metab. Pharmacokinet.*, **19**, 352—362 (2004).
20) Sato K., Sugibayashi K., Morimoto Y., *J. Pharm. Sci.*, **80**, 104—107 (1991).
21) Scientific Committee on Consumer Product, "Opinion on Safety on Nanomaterials in Cosmetic Products," 2007.
22) Lauer A. C., Lieb L. M., Ramachandran C., Flynn G. L., Weiner N. D., *Pharm. Res.*, **12**, 179—186 (1995).
23) Okamoto H., Yamashita F., Saito K., Hashida M., *Pharm. Res.*, **6**, 931—937 (1989).
24) Ogiso T., Shiraki T., Okajima K., Tanino T., Iwaki M., Wada T., *J. Drug Target*, **10**, 369—378 (2002).
25) Knorr F., Lademann J., Patzelt A., Sterry W., Blume-Peytavi U., Vogt A., *Eur. J. Pharm. Biopharm.*, **71**, 173—180 (2009).

Formulation Design and Photochemical Studies on Nanocrystal Solid Dispersion of Curcumin With Improved Oral Bioavailability

SATOMI ONOUE,[1] HARUKI TAKAHASHI,[1] YOHEI KAWABATA,[1] YOSHIKI SETO,[1] JUNYA HATANAKA,[1] BARBARA TIMMERMANN,[2] SHIZUO YAMADA[1]

[1]Department of Pharmacokinetics and Pharmacodynamics, Global Center of Excellence (COE) Program, School of Pharmaceutical Sciences, University of Shizuoka, 52-1 Yada, Suruga-ku, Shizuoka 422-8526, Japan

[2]Department of Medicinal Chemistry, School of Pharmacy, University of Kansas, Lawrence, Kansas 66045

Received 21 June 2009; revised 19 August 2009; accepted 31 August 2009

Published online 13 October 2009 in Wiley InterScience (www.interscience.wiley.com). DOI 10.1002/jps.21964

ABSTRACT: Considerable interest has been focused on curcumin due to its use to treat a wide variety of disorders, however, the therapeutic potential of curcumin could often be limited by its poor solubility, bioavailability, and photostability. To overcome these drawbacks, efficacious formulations of curcumin, including nanocrystal solid dispersion (CSD-Cur), amorphous solid dispersion (ASD-Cur), and nanoemulsion (NE-Cur), were designed with the aim of improving physicochemical and pharmacokinetic properties. Physicochemical properties of the prepared formulations were characterized by scanning/transmission electron microscope for morphological analysis, laser diffraction, and dynamic light scattering for particle size analysis, and polarized light microscope, powder X-ray diffraction and differential scanning calorimetry for crystallinity assessment. In dissolution tests, all curcumin formulations exhibited marked improvement in the dissolution behavior when compared with crystalline curcumin. Significant improvement in pharmacokinetic behavior was observed in the newly developed formulations, as evidenced by 12- (ASD-Cur), 16- (CSD-Cur), and 9-fold (NE-Cur) increase of oral bioavailability. Upon photochemical characterization, curcumin was found to be photoreactive and photodegradable in the solution state, possibly via type 2 photochemical reaction, whereas high photochemical stability was seen in the solid formulations, especially CSD-Cur. On the basis of these observations, taken together with dissolution and pharmacokinetic behaviors, CSD strategy would be efficacious to enhance bioavailability of curcumin with high photochemical stability. J Pharm Sci 99:1871–1881, 2010

Keywords: curcumin; solid dispersion; emulsion; absorption; photostability

INTRODUCTION

Curcumin [1,7-*bis*(4-hydroxy-3-methoxyphenyl)-1, 6-heptadiene-3,5-dione] is a naturally occurring hydrophobic polyphenol, derived from the rhizomes of turmeric (*Curcuma longa* L.).[1] It has been widely used as a yellow pigment to color food, drugs, and cosmetics, and it is also interesting from a medical point of view, because of its potential use for treatment of various chronic

Abbreviations used: ASD, amorphous solid dispersion; CD, cyclodextrin; CSD, nanocrystal solid dispersion; DLS, dynamic light scattering; DSC, differential scanning calorimetry; NBT, nitroblue tetrazolium; NE, nanoemulsion; PLM, polarized light microscope; RNO, *p*-nitrosodimethylaniline; ROS, reactive oxygen species; SEM, scanning electron microscope; TEM, transmission electron microscopy; UPLC, ultra-performance liquid chromatography; UV, ultra violet; XRPD, X-ray powder diffraction.

Correspondence to: Satomi Onoue (Telephone: 81-54-264-5633; Fax: 81-54-264-5635;
E-mail: onoue@u-shizuoka-ken.ac.jp)

Journal of Pharmaceutical Sciences, Vol. 99, 1871–1881 (2010)

diseases.[2] A growing body of experimental evidence suggests various beneficial pharmacological effects of curcumin, including anti-oxidant, anti-inflammatory, anti-carcinogenic, anti-bacterial, and anti-coagulant.[3–6] In spite of these attractive activities of curcumin, the therapeutic efficiency of curcumin has been highly limited, partly due to its low oral bioavailability (1% or much lower).[7,8] Curcumin was found to be poorly soluble in water, the maximum solubility of which in aqueous buffer (pH 5.0) was reported to be as low as 11 ng/mL.[9] The limited solubility of curcumin, as well as extensive systemic metabolism, could be responsible for the low bioavailability of curcumin after oral delivery.[10,11] In addition, curcumin in solution state could be sensitive to UV light, so that marked photochemical degradation could occur under UV exposure,[12] leading to the difficulty in its handling for clinical use.

A number of efforts have been made to design soluble formulations of curcumin, which include liposomal formulation,[13] curcumin–phospholipid complex,[10] curcumin–CD complex,[9,14] and micellar formulation.[15] So far, suitable delivery options have not been optimized, however, the use of CD strategies for solubilization led to a marked decrease in compound photostability.[9] In this context, there have been considerable interests in developing alternative oral delivery systems of curcumin with the aim of overcoming several drawbacks and enhancing its pharmacological effects. In general, different strategies such as salt formulation and particle size reduction have been commonly used in order to increase dissolution rates of poorly soluble drugs.[16] There are practical limitations with these techniques, however, and the desired bioavailability enhancement might not always be achieved. Attention has been drawn to solid dispersion systems, demonstrating the promising results in increasing bioavailability of poorly water-soluble drugs, in which the drug is dispersed in solid water-soluble matrices either molecularly or as fine particles.[17]

The main purpose of the present investigation is to develop soluble formulations of curcumin with enhanced bioavailability and photostability. Solid dispersion formulations of curcumin including crystalline and ASD were prepared as well as a NE and a liquid formulation for comparative purposes. Physicochemical properties of the formulations were characterized with emphasis on surface morphology, size distribution, crystallinity, thermal property, and dissolution behavior. As curcumin is susceptible to photodegradation, photochemical properties of curcumin formulations were assessed by a photostability study and a ROS assay as proposed in previous investigations.[18] Pharmacokinetic profiling of curcumin after oral administration of soluble formulations was carried out with the use of UPLC/ESI-MS.

MATERIALS AND METHODS

Chemicals

Curcumin was purchased from Sabinsa Japan Corporation (Tokyo, Japan). Hydroxypropyl cellulose SL (HPC-SL) and hydroxypropyl methylcellulose acetate succinate (HPMC-AS) were kindly provided from Shin-Etsu Chemical (Tokyo, Japan). Ammonium acetate, dimethyl sulfoxide (DMSO), dioxane, Polyethylene glycol 400 (PEG400), propylene glycol, sodium dodecyl sulfate (SDS), and Tween-80 were purchased from Wako Pure Chemical Industries (Osaka, Japan). Benzocaine was purchased from Tokyo Chemical Industry (Tokyo, Japan). All other chemicals were purchased from various commercial sources.

Preparation of Nanocrystal Solid Dispersion (CSD-Cur)

The wet-milled curcumin formulation was prepared with NanoMill®-01 system (Elan Drug Technologies, Dublin, Ireland). Briefly, 882.0 mg of curcumin was weighed and added to a 100 mL stainless chamber. Polystyrene beads (46.7 g) with diameter of 0.5 mm were placed into the chamber and 44.1 mL of 5 mg/mL HPC-SL solution with 0.2 mg/mL SDS was added. The curcumin colloidal suspension was micronized at 3600 rpm for 90 min with a NanoMill®-01 system in the chamber kept at 5°C. After micronization with the wet-milling process, the curcumin suspension was collected with a syringe and freeze-dried with freeze dryer FD-1000 (Tokyo Rikakikai, Tokyo, Japan).

Preparation of Amorphous Solid Dispersion (ASD-Cur)

Curcumin (200 mg) and HPMC-AS (800 mg) were dissolved in 90% (v/v) dioxane solution. The solution was mixed well and frozen at −80°C. The sample was freeze-dried with a freeze dryer LyoStar II (SP Industries, Warminster, PA). After

drying, the sample was sieved with two different mesh sizes of sieves (1 and 2 mm).

Preparation of Nanoemulsion Formulation (NE-Cur)

For the preparation of an emulsion preconcentrate, curcumin (6 mg) was dissolved in a solvent mixture consisting of 200 μL of PEG400, 100 μL of propylene glycol, 50 μL of ethanol, and 10 μL of Tween-80, and sonicated thoroughly at room temperature. Upon contact with the aqueous medium, an emulsion preconcentrate spontaneously formed as a fine dispersion.

Polarized Light Microscope (PLM)

PLM images were taken using an ECLIPSE E600 POL microscope (Nikon, Tokyo, Japan). Curcumin samples were examined under various conditions including differential interference contrast, slightly uncrossed polars, and using a red wave compensator.

Scanning Electron Microscope (SEM)

Representative SEM images of curcumin solid formulations were taken using SEM, VE-7800 (Keyence, Osaka, Japan), without Au or Pt coating. For the SEM observations, each sample was fixed on an aluminum sample holder using a double-sided carbon tape.

Transmission Electron Microscopy (TEM)

An aliquot (2 μL) of the curcumin liquid formulation was placed on a carbon-coated Formvar 200 mesh nickel grid. The sample was allowed to stand for 15–30 s, and then any excess of solution was removed by blotting. The samples were negatively stained with 2% (w/v) uranyl acetate and allowed to dry. The samples were then visualized under as H-7600 transmission electron microscope (Hitachi, Tokyo, Japan) operating at 75 kV.

Laser Diffraction

Particle size of curcumin was measured by a laser diffraction scattering method using a Microtrac HRA X-100 (Nikkiso, Tokyo, Japan). For measurement, curcumin was suspended in distilled water. The particle size distribution was expressed as the volume median diameter and SPAN factor defined as $\text{SPAN} = (d_{90} - d_{10})/d_{50}$, where d_{10}, d_{50}, and d_{90} are the particle diameters at 10%, 50%, and 90% of the cumulative volume, respectively. A high SPAN value indicates a wide size distribution.

Dynamic Light Scattering (DLS)

Particle size of wet-milled or emulsified curcumin was measured by DLS method using a N5 submicron particle size analyzer (Beckman Coulter, Tokyo, Japan). For measurement, one drop of curcumin suspension was diluted with 4 mL distilled water and dispersed homogeneously. Mean diameter was calculated using the photon correlation from light scattering. All measurements were performed at 25°C at a measurement angle of 90°. The size distribution, which was calculated by histogram analysis of scattering intensity, was evaluated at cumulative values of 10%, 50%, and 90%.

X-Ray Powder Diffraction (XRPD)

The powder X-ray diffraction pattern was collected with D8 ADVANCE (Bruker AXS GmbH, Karlsruhe, Germany) with Cu Kα radiation generated at 40 mA and 35 kV. Data were obtained from 4° to 40° (2θ) at a step size of 0.014° and scanning speed of 4°/min.

Thermal Analysis

DSC was performed using a DSC Q1000 (TA instruments, New Castle, DE). The DSC thermograms were collected in an aluminum close-pan system using a sample weight of ca. Three milligrams and a heating rate of 5°C/min with nitrogen purge at 70 mL/min. The temperature axis was calibrated with indium (ca. 5 mg, 99.999% pure, onset at 156.6°C).

Dissolution Test

Dissolution tests were carried out for 180 min in 900 mL distilled water containing 0.05% Tween-80 with constant stirring of 200 rpm in a dissolution test apparatus DE-1S (Tokyo Rikakikai) at 37°C. One milligram of the curcumin formulation was weighed to the dissolution vessel. Samples

were collected at the indicated periods (5, 10, 20, 30, 40, 60, 90, 120, and 180 min) and centrifuged at 15,000 *g* to remove insoluble materials. For determination of curcumin concentration in the supernatant, fluorescence (excitation, 430 nm and emission, 550 nm) of each supernatant (200 μL) in a 96-well microplate was measured with a microplate reader, Safire (Tecan, Männedorf, Switzerland).

Animals and Drug Administration

Male Sprague–Dawley rats (Japan SLC, Shizuoka, Japan), weighing 357 ± 59 g, were housed two per cage in the laboratory with free access to food and water, and maintained on a 12-h dark/light cycle in a room with controlled temperature (24 ± 1°C) and humidity (55 ± 5%). All the procedures used in the present study were conducted according to the guidelines approved by the Institutional Animal Care and Ethical Committee of the University of Shizuoka. For oral administration, each curcumin formulation was suspended in distilled water. Rats were fasted for ~18 h before drug administration, and received orally curcumin (100 mg/kg body weight) or curcumin formulations (20 mg curcumin/kg body weight). For intravenous injection, 2 mg of curcumin were dissolved in 1 mL of DMSO, and 100 μL of DMSO solution of curcumin was diluted to 1 mL with PBS containing 0.5% (v/v) Tween-80 (final concentration of curcumin, 200 μg/mL). The curcumin solution was filtered through a 0.22 μm membrane filter (Millipore, Tokyo, Japan), and injected intravenously to rats (0.5 mg/kg body weight).

Plasma Concentration of Curcumin

Blood samples were taken in a volume of 200 μL from the tail vein in the indicated periods after oral administration of curcumin or curcumin formulations. The blood samples were centrifuged at 10,000 *g* to prepare plasma samples. The plasma samples were kept frozen at below −20°C until they were analyzed. Curcumin concentrations in plasma were estimated by internal standard method using UPLC/ESI-MS. Briefly, 250 μL of acetonitrile and internal standard (benzocaine) were added to 100 μL of plasma sample and centrifuged at 2000 rpm for 1 min. The supernatant was analyzed by Waters Acquity UPLC system (Waters, Milford, MA), that include the binary solvent manager, sample manager, column compartment, and SQD connected with MassLynx software. An Acquity UPLC BEH C 18 column (particle size: 1.7 μm, column size: 2.1 mm × 50 mm; Waters), also from Waters, was used, and column temperature was maintained at 40°C. The samples were separated using a gradient mobile phase consisting of 5 mM ammonium acetate (A) and acetonitrile (B) with the flow rate of 0.25 mL/min, and the retention time of curcumin was 3.1 min. The gradient condition of mobile phase was 0–0.5 min, 30% B; and 0.5–3.5 min, 30–70% B.

Photostability Study

Each curcumin formulation was stored in an Atlas Suntest CPS+ solar simulator (Atlas Material Technology LLC, Chicago, IL), equipped with a xenon arc lamp. UV special filter and window glass filter were installed to adapt the spectrum of the artificial light source to natural daylight. The irradiation test was carried out at 25°C with an irradiance of 750 W/m^2. Each curcumin formulation was stored in a clear glass vial and irradiated with UVA/B light for 1 h (2700 kJ/m^2), and the remaining curcumin in the sample was determined by UPLC/ESI-MS, as described in Plasma Concentration of Curcumin Section.

Reactive Oxygen Species (ROS) Assay

ROS assay on curcumin solution was carried out according to our previous reports with some modifications.[18,19] Briefly, singlet oxygen was measured in an aqueous solution by spectrophotometrically monitoring the bleaching of RNO at 440 nm using imidazole as a selective acceptor of singlet oxygen. Samples containing the compounds under examination, RNO (50 μM) and imidazole (50 μM) in 20 mM sodium phosphate buffer (NaPB, pH 7.4) were irradiated with UVA/B (250 W/m^2) for the indicated periods, followed by measurements of UV absorption at 440 nm with a SpectraMax plus 384 microplate spectrophotometer (Molecular Devices, Kobe, Japan). For measurement of superoxide anion, samples containing the compounds under examination and NBT (50 μM) in 20 mM NaPB were irradiated with UVA/B (250 W/m^2), and the reduction of NBT was measured by the increase of the absorbance at 560 nm, using a SpectraMax plus 384 microplate spectrophotometer.

Statistical Analysis

For statistical comparisons, a one-way analysis of variance (ANOVA) with the pairwise comparison by Fisher's least significant difference procedure was used. A p-value of <0.05 was considered significant for all analyses.

RESULTS AND DISCUSSION

Solid Dispersions of Curcumin

Solid dispersion can be defined as a distribution of active ingredients in molecular, amorphous, and/or microcrystalline forms surrounded by inert carriers.[17] In the present investigation, two types of solid dispersion were prepared, such as CSD- and ASD-Cur, and both solid dispersions appeared as light yellow, dry, and fine powder. Representative SEM and PLM images of solid dispersions are shown in Figure 1. In SEM images, crystalline curcumin showed the particles to be predominantly dispersed and irregularly shaped, with sizes ranging over about 10–100 μm (Fig. 1A-I), whereas the solid dispersions exhibited the appearance of typical, flaky freeze-dried material (Fig. 1B-I and C-I). These observations revealed clear changes in the morphology of the powder particles due to the evident formation of solid dispersions, and there seemed to be marked increase in the surface area of the material when compared with curcumin alone. According to PLM appearance, intense birefringence was observed in curcumin (Fig. 1A-II), suggesting its high crystallinity. In contrast, solid dispersions, even CSD-Cur, showed no birefringence (Fig. 1B-II and C-II) that could be reasonable for the theoretical physical state of ASD-Cur, but not for CSD-Cur. The lack of birefringence in CSD-Cur might be caused by marked reduction in particle size of crystalline curcumin down to the submicron range. Afterwards, the particle size of curcumin and CSD-Cur suspended in water was evaluated by laser diffraction and DLS, respectively (Fig. 2).

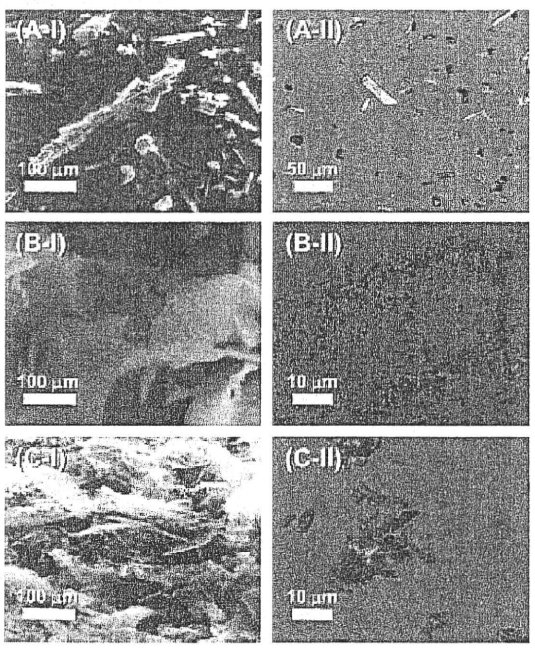

Figure 1. Microscopic images of curcumin samples, including curcumin (A), CSD-Cur (B), and ASD-Cur (C). Surface morphology of each sample was evaluated by scanning electron microscopy (left) and polarized light microscopy (right).

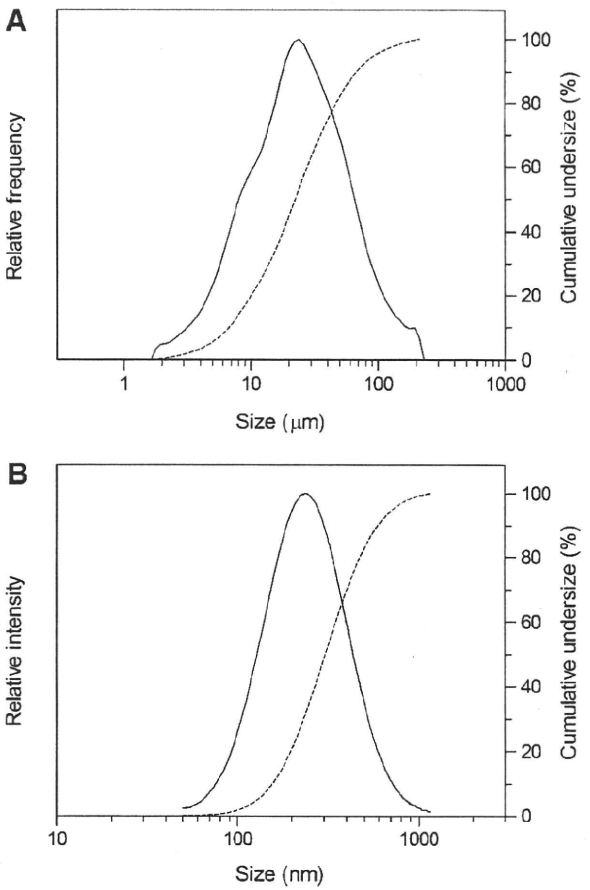

Figure 2. Size distributions of curcumin and CSD-Cur. Particle size of curcumin (A) and CSD-Cur (B) was determined by laser diffraction and dynamic light scattering method, respectively. Solid line, relative frequency/intensity; and dotted line, cumulative undersize.

The mean diameter of crystalline curcumin (A) was calculated to be 22 μm with SPAN factor of 2.7, and CSD-Cur suspension (B) exhibited the mean diameter of as low as 250 nm, indicating that wet-milling of curcumin led to ca. 10^2-fold reduction of particle size. The polydispersity index of CSD-Cur suspension ranged from 0.3 to 0.4, suggesting that the milled particles were moderately homogeneous.

Further characterization on physicochemical properties of curcumin formulations was made with use of XRPD and DSC. The XRPD pattern of crystalline curcumin indicated several characteristic peaks, and the similar diffraction pattern was also seen in CSD-Cur (Fig. 3A). This could be indicative of high crystallinity of curcumin in the formulation, and the crystal habit might be attributed to the slight transition of diffraction pattern between crystalline curcumin and CSD-Cur. In contrast, ASD-Cur was found to be amorphous, as indicated by a halo diffraction pattern, and this was consistent with the PLM observation. In addition to the XRPD data, the thermal behavior of drug formulations are also of importance in pharmaceutical technologies, since the obtained information such as melting, recrystallization, decomposition, or a change in heat capacity could help to ascertain the physicochemical status of the entrapped drug inside the excipient. The DSC thermograms of curcumin formulations are provided in Figure 3B. Both crystalline curcumin and CSD-Cur produced an intense melting endotherm at ca. 180°C, supporting the results obtained during XRPD analysis. However, ASD-Cur did not show any thermal event in the examined temperature range (30–250°C), and these data suggested that curcumin in ASD-Cur exists in an amorphous form as observed in other assessments. On the basis of morphological observations and physicochemical characterization, amorphous, and crystal solid dispersions of curcumin were successfully developed with the aim of controlling the molecular properties of curcumin.

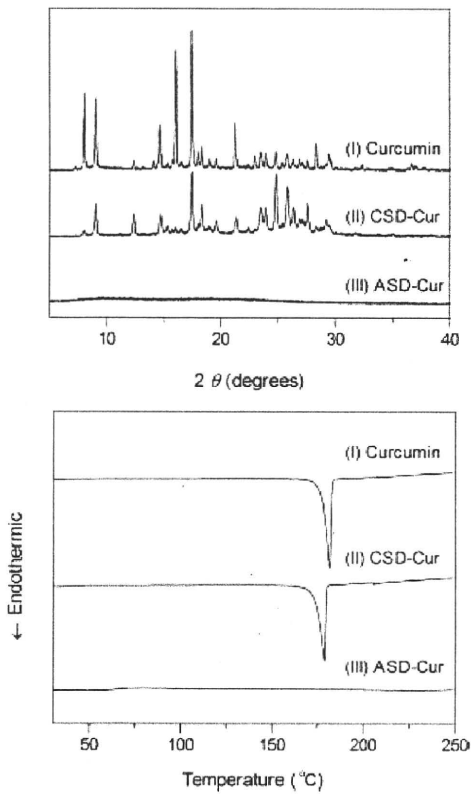

Figure 3. Physicochemical characterization of curcumin samples, including (I) curcumin (crystalline), (II) CSD-Cur, and (III) ASD-Cur. (A) Powder X-ray diffraction patterns and (B) DSC thermograms.

Nanoemulsion Formulation of Curcumin

For improvement of solubility and bioavailability of poorly soluble drugs, one of the most popular and commercially viable formulation approaches is emulsification. Recently, the preparation of submicron emulsions, called NE or mini-emulsions, has emerged as a promising alternative dosage form,[20] because of their long-term stability, ease of preparation, and high solubilization of drug molecules. As they have found wide application in oral drug delivery to enhance the solubility and bioavailability of the lipophilic drugs, a NE-Cur was prepared to compare its physicochemical and pharmacokinetic behaviors to other curcumin formulations in the present study. An emulsion preconcentrate of curcumin was prepared consisting of curcumin, PEG400, Tween-80, and propylene glycol which formed a spontaneous and fine dispersion upon contact with the aqueous media. Morphology of NE-Cur was characterized by TEM observation, indicating that all the NE particles were evenly distributed and spherical (Fig. 4A). The emulsion preconcentrate of curcumin formed a NE where particle sizes were less than at least 500 μm. No precipitation was observed at 40°C for at least 2 h after emulsification (data not shown). In addition, NE-Cur was subjected to DLS analysis, and the average particle size of NE-Cur was found to be 196 nm

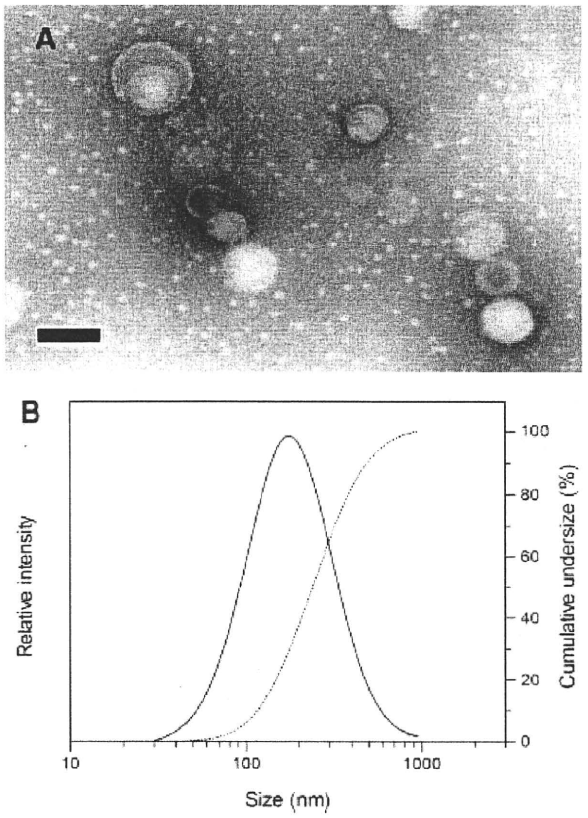

Figure 4. Nanoemulsion formulation of curcumin. (A) Transmission electron microscopic image of NE-Cur, suspended in water. Scale bar = 100 nm. (B) Size distribution of NE-Cur in water, as determined by dynamic light scattering. Solid line, relative intensity; and dotted line, cumulative undersize.

(Fig. 4B). The particle size was approximately the same as the diameters observed by TEM. Thus, a nanoemulsified dispersion of curcumin was produced by the addition of an emulsion preconcentrate into the aqueous solution.

Dissolution Properties of Curcumin Formulations

To demonstrate the improved solubility of each curcumin formulation, the drug dissolution profiles of crystalline curcumin, CSD-Cur, ASD-Cur, and NE-Cur were examined up to 180 min (Fig. 5). Of all curcumin formulations tested, NE-Cur showed the fastest dispersion with formation of NE as determined by DLS, although dissolution of crystalline curcumin into water was found to be much slower than the tested curcumin formulations. Both solid dispersions of curcumin exhibited the improved dissolution/dispersion behavior, as evidenced by ca.

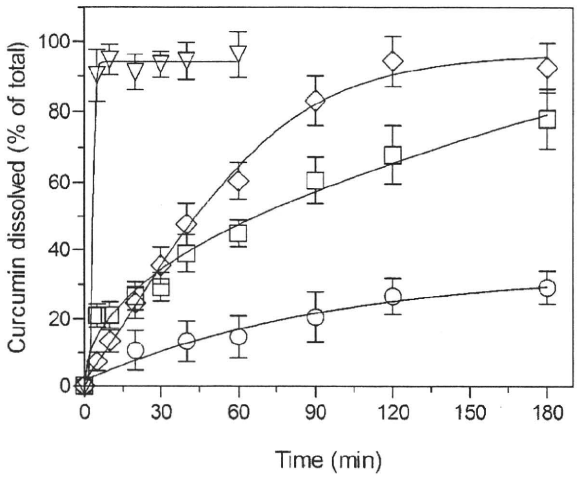

Figure 5. Dissolution profiles of curcumin samples, differently treated in deionized water. ○, curcumin (crystalline); □, CSD-Cur; ◇, ASD-Cur; and ▽, NE-Cur. Each bar represents mean ± SE of three independent experiments.

95% (ASD-Cur) and 80% (CSD-Cur) release at 180 min. According to the dissolution curve, the dissolution rates of curcumin, ASD- and CSD-Cur were estimated to be $0.16\,h^{-1}$ (95% confidence interval; 95% CI, 0.13–0.19), $0.93\,h^{-1}$ (95% CI, 0.90–0.97), and $0.60\,h^{-1}$ (95% CI, 0.53–0.68), respectively. These observations were consistent with previous reports, showing that formulation of poorly soluble drugs as solid dispersions could lead to a marked improvement in the dissolution properties.[21] It is well established that for poorly water-soluble drugs, even a small increase in their dissolution rate could result in a large increase in bioavailability, as the bioavailability of a poorly soluble drug is largely dependent on its dissolution rate.[22] Based on the dissolution profiles, as well as the physicochemical characteristics of the newly developed curcumin formulations, solid dispersion approach might be one of potential options for oral preparations because of their improved dissolution properties in water.

Pharmacokinetic Behaviors of Curcumin Formulations

The observations of the dissolution properties of curcumin formulations prompted us to clarify the possible improvement in the bioavailability of curcumin by the assessment of the pharmacokinetic behaviors of curcumin formulations in rats. Figure 6 shows the blood concentration–time

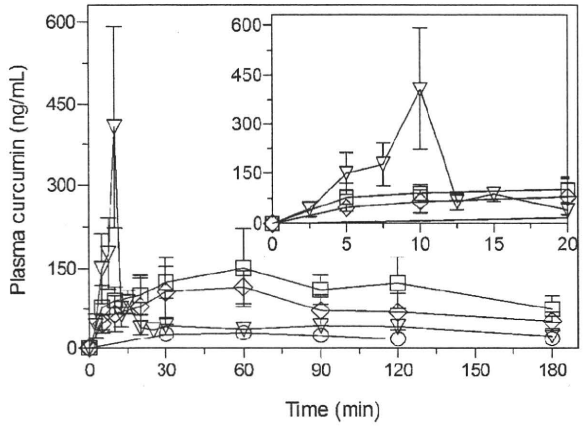

Figure 6. Plasma curcumin concentrations in rats after oral administration of curcumin formulations. ○, curcumin (crystalline) at 100 mg/kg body weight of rat; □, CSD-Cur at 20 mg/kg; ◇, ASD-Cur at 20 mg/kg; and ▽, NE-Cur at 20 mg/kg. The inset highlights the concentration values obtained after oral administration of curcumin formulations. Data represent mean ± SE of 4–5 experiments.

profiles of curcumin in rats after an oral administration of the newly developed curcumin formulations (20 mg curcumin/kg) and curcumin (100 mg/kg), and relevant pharmacokinetic parameters including C_{max}, T_{max}, $T_{1/2}$, AUC_{0-inf}, and absolute bioavailability as listed in Table 1. Oral administration of NE-Cur (20 mg/kg curcumin) resulted in a rapid elevation of curcumin blood levels up to C_{max} 451 ng/mL within 10 min, and the AUC value was calculated to be 20 μg/mL min. The plasma concentration of curcumin decreased rapidly with elimination half-life of 39 min. On the contrary, curcumin levels in the blood were found to be very low when the curcumin (100 mg/kg) was administered orally, and the C_{max} and AUC values were 35 ng/mL and 11 μg/mL min, respectively. Thus, there appeared to be a marked enhancement in C_{max} of curcumin with the use of NE technology, whereas NE-Cur exhibited much faster elimination than curcumin. Generally, curcumin undergoes extensive metabolism, mainly conjugation reaction like sulfation and glucuronidation, in the liver and intestinal wall.[23] So, rapid systemic elimination or clearance of curcumin was attributable to the rapid metabolism. Although curcumin is remarkably well tolerated in animals[24] and humans,[25] a high concentration of curcumin could stimulate the apoptotic signaling pathways in several tissues.[26] In this context, the NE approach to curcumin formulation might not be suitable because of its rapid elimination and the transient high levels of curcumin in plasma that could possibly lead to its limited duration of action and concomitant toxic risk. With respect to solid dispersions, CSD- and ASD-Cur exhibited an improved pharmacokinetic behavior as compared to crystalline curcumin. Both solid dispersions (20 mg curcumin/kg) were three- to fivefold higher in C_{max} and AUC values of plasma curcumin levels than curcumin (100 mg/kg), whereas similar T_{max} and half-lives were observed for curcumin and solid dispersions. Upon these findings, both solid dispersion formulations of curcumin could provide wider therapeutic safety margins when compared to NE-Cur. As shown in Table 1, absolute bioavailability of curcumin and its formulations were calculated to be 0.9% (curcumin), 7.9% (NE-Cur), 10.7% (ASD-Cur), and 14.3% (CSD-Cur) on the basis of AUC value of intravenously administered curcumin (0.5 mg/kg, data not shown). Rapid elimination of curcumin, possibly due to extensive metabolism, was seen in rats treated with NE-Cur, although both SD formulations exhibited the prolonged retention in blood after oral administration. According to the results from dissolution study, both SD approaches for curcumin allowed to obtain a prolonged release of curcumin, as compared with NE-Cur. The marked differences in pharmacokinetic behavior between SD and NE

Table 1. Pharmacokinetic Parameters of Curcumin Formulations Following Oral Administration

Formulations	Dose (mg/kg)	C_{max} (ng/mL)	T_{max} (min)	$T_{1/2}$ (min)	AUC_{0-inf} (μg/mL min)	BA (%)
Curcumin (crystalline)	100	35 ± 8.0	80 ± 10	207 ± 94	11.0 ± 0.5	0.9
CSD-Cur	20	194 ± 58	55 ± 24	173 ± 68	36.2 ± 10.8	14.3
ASD-Cur	20	147 ± 53	60 ± 12	221 ± 54	27.1 ± 6.7	10.7
NE-Cur	20	451 ± 166	8.7 ± 2.5	39 ± 10	20.0 ± 6.4	7.9

C_{max}, maximum concentration; T_{max}, time to maximum concentration; $T_{1/2}$, half-life; and AUC_{0-inf}, area under the curve of plasma concentration versus time from $t = 0$ to $t = \infty$ after administration.

Values are expressed as means ± SE from 4–5 experiments.

formulations might be partly attributed to the different release behavior. Upon these findings, solid dispersion strategies, and especially crystal solid dispersion, might be a simple and efficacious method to improve the pharmacokinetic behavior of curcumin.

Currently, curcumin is under active investigation for its clinical benefit, although clinical trials are still in relatively early phases.[27] In a clinical study with healthy volunteers where curcumin was administered as a single daily oral dose ranging from 0.5 to 12 g,[28] low levels of curcumin were detected only in the serum of volunteers receiving high doses of curcumin (10 or 12 g/day). The use of such a large dose in a bulky tablet or alternative dosage options would not always be an acceptable form of delivery to patients. On the basis of the oral bioavailability data on curcumin and its formulations in rats, there is a probability that the use of solid dispersion approaches to curcumin as was demonstrated here could reduce the daily oral dose of curcumin.

Photochemical Behavior of Curcumin Formulations

According to the first law of photochemistry, alternatively referred to as the Grotthus–Draper law,[29] chemicals could be activated by the absorption of photon energy, if those chemicals have UV spectral patterns which overlap with the sunlight spectrum. Curcumin showed strong absorption in the UVA/VIS range,[30] so that curcumin may absorb photon energy and be excited under exposure to sunlight. Previously, our group proposed that a ROS assay system for monitoring ROS generation from test compounds irradiated with UVA/B could be predictive of the photoreactivity and/or phototoxic potential of drug candidates.[18] In the present study, the ROS assay was carried out on curcumin to assess its photochemical behavior. According to the results of ROS assay for curcumin at 20 μM (Fig. 7A), generation of ROS, especially singlet oxygen, from curcumin irradiated with UVA/B were observed, whereas curcumin kept in the dark did not show any RNO bleaching or NBT reduction (data not shown). In comparison with ROS data on other photosensitive chemicals, the ability of curcumin to generate singlet oxygen and superoxide was found to be similar to that of sulfamethoxazole (singlet oxygen, $\Delta A_{440\,nm} \times 10^3$: 66; and superoxide, $\Delta A_{560\,nm} \times 10^3$: 4) at the concentration of 20 μM; the phototoxicity of sulfamethoxazole has

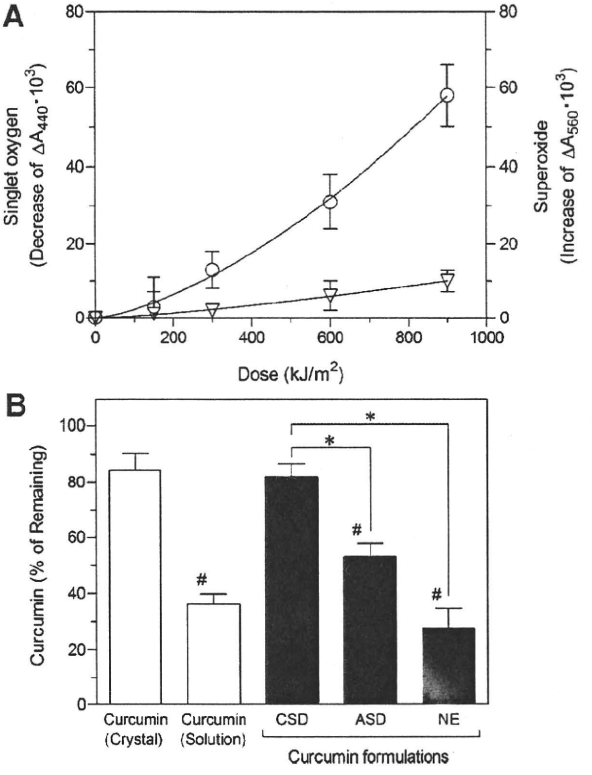

Figure 7. Photochemical properties of curcumin formulations. (A) Generation of singlet oxygen (○) and superoxide (▽) from curcumin irradiated with UVA/B light. Curcumin was dissolved in 20 mM NaPB (pH 7.4) at the concentration of 20 μM, and then exposed to the indicated dose of UVA/B. Data represent mean ± SE of four experiments. (B) Light-induced degradation of curcumin samples, including crystalline curcumin, curcumin solution (DMSO), CSD-Cur, ASD-Cur, and NE-Cur. Each curcumin formulation was exposed to UVA/B (750 W/m^2) for 1 h, and the potency (% of remaining) of curcumin was determined by UPLC/ESI-MS analysis. $^{\#}p < 0.01$ with respect to crystalline curcumin; and $^{*}p < 0.01$ between indicated groups.

been well characterized in *in vitro* and *in vivo* models.[31] Based on the results of the ROS assay, as well as UV spectral data, curcumin was identified to have photoreactive potential through the type II photochemical reactions, possibly leading to photodegradation.

For further investigation of the photochemical responses of curcumin, photochemical stability of each curcumin formulation was assessed. Exposure of curcumin, dissolved in DMSO, and NE-Cur to simulated sunlight at the indicated irradiance resulted in gradual degradation of curcumin, and UPLC/ESI-MS analysis indicated ca. 70% decrease of potency after UV irradiation

(2700 kJ/m^2) (Fig. 7B). On the contrary, crystalline curcumin was found to be photochemically stable with no color changes after UV irradiation (450 kJ/m^2, data not shown). Only 15% degradation was observed when crystalline curcumin was exposed to very intense UV light with total irradiation energy of 2700 kJ/m^2. These observations could be consistent with our previous observation, demonstrating that photodegradation of a crystalline dihydropyridine derivative was much slower than in its solution state.[32] With respect to other solid formulation, ca. 50% reduction of potency was observed in ASD-Cur at the same irradiation condition (2700 kJ/m^2), although CSD-Cur exhibited similar photostability as crystalline curcumin, as evidenced by 17% degradation. Generally, crystalline chemicals tend to be more stable as compared to their amorphous forms, and this could be a part of the reasons for the differences observed in photostability between ASD-Cur and CSD-Cur. Thus, solid dispersions of curcumin, in particular CSD-Cur, could be photochemically stable while in the solid state, however, once solubilized, they could be susceptible to photochemical degradation under intense UVA/B irradiation. On the basis of these findings, taken together with dissolution and pharmacokinetic profiles, crystal solid dispersion approaches would be effective for developing a water-soluble formulation of curcumin with improved bioavailability and high photostability.

CONCLUSION

In the present investigation, the water-soluble formulations of curcumin, including crystal/amorphous solid dispersions and NE, were prepared, and they showed rapid dissolution/dispersion behavior as compared to crystalline curcumin. The mean particle size of curcumin in crystal solid dispersion, prepared by wet-milling and subsequent freeze-drying, was found to be ca. 250 nm with small polydispersity index, suggesting that the powder formulation contains nanosized crystal of curcumin. There appeared to be marked improvement in pharmacokinetic behavior of the newly developed formulations, as evidenced by 12- (ASD-Cur), 16- (CSD-Cur), and 9-fold (NE-Cur) increase in oral bioavailability. Although curcumin in the solution state was found to be photoreactive and photodegradable, high photochemical stability was seen in the crystal solid dispersion of curcumin and crystalline curcumin. Upon these observations on stability, dissolution, and pharmacokinetic behaviors, crystal solid dispersion approach would be efficacious to enhance bioavailability of curcumin with high photostability, and this could be advantageous for the safe therapy of inflammatory or other chronic diseases.

ACKNOWLEDGMENTS

We wish to thank Mr. Masanori Ochi, University of Shizuoka, for excellent technical assistance throughout this work. This work was supported in part by a grant-in-aid for Young Scientists (B) (No. 20790103; S. Onoue) from the Ministry of Education, Culture, Sports, Science and Technology, and Research and Development Projects for Application in Promoting New Policy of Agriculture Forestry and Fisheries from the Ministry of Agriculture, Forestry and Fisheries.

REFERENCES

1. Lantz RC, Chen GJ, Solyom AM, Jolad SD, Timmermann BN. 2005. The effect of turmeric extracts on inflammatory mediator production. Phytomedicine 12:445–452.
2. Funk JL, Oyarzo JN, Frye JB, Chen G, Lantz RC, Jolad SD, Solyom AM, Timmermann BN. 2006. Turmeric extracts containing curcuminoids prevent experimental rheumatoid arthritis. J Nat Prod 69: 351–355.
3. Ammon HP, Wahl MA. 1991. Pharmacology of Curcuma longa. Planta Med 57:1–7.
4. Reddy AC, Lokesh BR. 1992. Studies on spice principles as antioxidants in the inhibition of lipid peroxidation of rat liver microsomes. Mol Cell Biochem 111:117–124.
5. Shukla Y, Arora A, Taneja P. 2002. Antimutagenic potential of curcumin on chromosomal aberrations in Wistar rats. Mutat Res 515:197–202.
6. Billerey-Larmonier C, Uno JK, Larmonier N, Midura AJ, Timmermann B, Ghishan FK, Kiela PR. 2008. Protective effects of dietary curcumin in mouse model of chemically induced colitis are strain dependent. Inflamm Bowel Dis 14:780–793.
7. Pan MH, Huang TM, Lin JK. 1999. Biotransformation of curcumin through reduction and glucuronidation in mice. Drug Metab Dispos 27:486–494.
8. Yang KY, Lin LC, Tseng TY, Wang SC, Tsai TH. 2007. Oral bioavailability of curcumin in rat and the herbal analysis from Curcuma longa by LC-MS/MS. J Chromatogr B Analyt Technol Biomed Life Sci 853:183–189.

9. Tonnesen HH, Masson M, Loftsson T. 2002. Studies of curcumin and curcuminoids. XXVII. Cyclodextrin complexation: Solubility, chemical and photochemical stability. Int J Pharm 244:127–135.
10. Maiti K, Mukherjee K, Gantait A, Saha BP, Mukherjee PK. 2007. Curcumin-phospholipid complex: Preparation, therapeutic evaluation and pharmacokinetic study in rats. Int J Pharm 330:155–163.
11. Sharma RA, Gescher AJ, Steward WP. 2005. Curcumin: The story so far. Eur J Cancer 41:1955–1968.
12. Tonnesen HH, Karlsen J, van Henegouwen GB. 1986. Studies on curcumin and curcuminoids. VIII. Photochemical stability of curcumin. Z Lebensm Unters Forsch 183:116–122.
13. Chen C, Johnston TD, Jeon H, Gedaly R, McHugh PP, Burke TG, Ranjan D. 2009. An in vitro study of liposomal curcumin: Stability, toxicity and biological activity in human lymphocytes and Epstein-Barr virus-transformed human B-cells. Int J Pharm 366:133–139.
14. Tomren MA, Masson M, Loftsson T, Tonnesen HH. 2007. Studies on curcumin and curcuminoids XXXI. Symmetric and asymmetric curcuminoids: Stability, activity and complexation with cyclodextrin. Int J Pharm 338:27–34.
15. Letchford K, Liggins R, Burt H. 2008. Solubilization of hydrophobic drugs by methoxy poly(ethylene glycol)-block-polycaprolactone diblock copolymer micelles: Theoretical and experimental data and correlations. J Pharm Sci 97:1179–1190.
16. Serajuddin AT. 1999. Solid dispersion of poorly water-soluble drugs: Early promises, subsequent problems, and recent breakthroughs. J Pharm Sci 88:1058–1066.
17. Chiou WL, Riegelman S. 1971. Pharmaceutical applications of solid dispersion systems. J Pharm Sci 60:1281–1302.
18. Onoue S, Tsuda Y. 2006. Analytical studies on the prediction of photosensitive/phototoxic potential of pharmaceutical substances. Pharm Res 23:156–164.
19. Onoue S, Kawamura K, Igarashi N, Zhou Y, Fujikawa M, Yamada H, Tsuda Y, Seto Y, Yamada S. 2008. Reactive oxygen species assay-based risk assessment of drug-induced phototoxicity: Classification criteria and application to drug candidates. J Pharm Biomed Anal 47:967–972.
20. Azeem A, Rizwan M, Ahmad FJ, Iqbal Z, Khar RK, Aqil M, Talegaonkar S. 2009. Nanoemulsion components screening and selection: A technical note. AAPS PharmSciTech 10:69–76.
21. Ren F, Jing Q, Tang Y, Shen Y, Chen J, Gao F, Cui J. 2006. Characteristics of bicalutamide solid dispersions and improvement of the dissolution. Drug Dev Ind Pharm 32:967–972.
22. Lobenberg R, Amidon GL. 2000. Modern bioavailability, bioequivalence and biopharmaceutics classification system. New scientific approaches to international regulatory standards. Eur J Pharm Biopharm 50:3–12.
23. Anand P, Kunnumakkara AB, Newman RA, Aggarwal BB. 2007. Bioavailability of curcumin: Problems and promises. Mol Pharm 4:807–818.
24. Shankar TN, Shantha NV, Ramesh HP, Murthy IA, Murthy VS. 1980. Toxicity studies on turmeric (Curcuma longa): Acute toxicity studies in rats, guineapigs & monkeys. Indian J Exp Biol 18:73–75.
25. Soni KB, Kuttan R. 1992. Effect of oral curcumin administration on serum peroxides and cholesterol levels in human volunteers. Indian J Physiol Pharmacol 36:273–275.
26. Joe B, Vijaykumar M, Lokesh BR. 2004. Biological properties of curcumin-cellular and molecular mechanisms of action. Crit Rev Food Sci Nutr 44: 97–111.
27. Hatcher H, Planalp R, Cho J, Torti FM, Torti SV. 2008. Curcumin: From ancient medicine to current clinical trials. Cell Mol Life Sci 65:1631–1652.
28. Lao CD, Ruffin MTT, Normolle D, Heath DD, Murray SI, Bailey JM, Boggs ME, Crowell J, Rock CL, Brenner DE. 2006. Dose escalation of a curcuminoid formulation. BMC Complement Altern Med 6:10.
29. Wondrak GT, Jacobson MK, Jacobson EL. 2006. Endogenous UVA-photosensitizers: Mediators of skin photodamage and novel targets for skin photoprotection. Photochem Photobiol Sci 5:215–237.
30. Ortica F, Rodgers MA. 2001. A laser flash photolysis study of curcumin in dioxane-water mixtures. Photochem Photobiol 74:745–751.
31. Jung J, Kim Y, Kim J, Jeong DH, Choi K. 2008. Environmental levels of ultraviolet light potentiate the toxicity of sulfonamide antibiotics in Daphnia magna. Ecotoxicology 17:37–45.
32. Onoue S, Igarashi N, Yamauchi Y, Murase N, Zhou Y, Kojima T, Yamada S, Tsuda Y. 2008. In vitro phototoxicity of dihydropyridine derivatives: A photochemical and photobiological study. Eur J Pharm Sci 33:262–270.

European Journal of Pharmaceutical Sciences 39 (2010) 256–262

Contents lists available at ScienceDirect

European Journal of Pharmaceutical Sciences

journal homepage: www.elsevier.com/locate/ejps

Novel crystalline solid dispersion of tranilast with high photostability and improved oral bioavailability

Yohei Kawabata[a], Kiyoshi Yamamoto[a], Kazuhiro Debari[b], Satomi Onoue[a,*], Shizuo Yamada[a]

[a] Department of Pharmacokinetics and Pharmacodynamics and Global Center of Excellence (COE) Program, School of Pharmaceutical Sciences, University of Shizuoka, 52-1 Yada, Suruga-ku, Shizuoka 422-8526, Japan
[b] Laboratory of Electron Microscopy, Showa University School of Medicine, Shinagawa, Tokyo 142-8555, Japan

ARTICLE INFO

Article history:
Received 11 September 2009
Received in revised form
17 November 2009
Accepted 17 December 2009
Available online 28 December 2009

Keywords:
Tranilast
Solid dispersion
Dissolution
Photostability
Absorption

ABSTRACT

Tranilast (TL) is an anti-allergic agent and widely used in the clinical treatment of bronchial asthma, atopic rhinitis, atopic dermatitis and keloids. However, therapeutic potential of TL could be partly limited because of its poor solubility, bioavailability, and photostability. To overcome these drawbacks, crystalline solid dispersion of TL (CSD/TL) was prepared by wet-milling technique with aim of improving physicochemical and pharmacokinetic properties. Physicochemical properties of the formulations prepared were characterized by laser diffraction and dynamic light scattering for particle size analysis, scanning electron microscope for morphological analysis, and powder X-ray diffraction and differential scanning calorimetry for crystallinity assessment. TL particles in CSD/TL appeared to be crystalline with diameter of 122 nm, and CSD/TL exhibited marked improvement in the dissolution behavior as compared to crystalline TL. Under irradiation of UVA/B (250 W/m^2), solution and amorphous solid dispersion of TL were found to be highly photodegradable, whereas high photochemical stability was seen in CSD/TL. After oral administration of CSD/TL, enhanced TL exposure was observed with increase of C_{max} and AUC by 60- and 32-fold, respectively, as compared to crystalline TL. According to these observations, taken together with dissolution and pharmacokinetic behaviors, crystalline solid dispersion strategy would be efficacious to enhance bioavailability of TL with high photochemical stability.

1. Introduction

Tranilast (TL), *N*-(3,4-dimethoxycinnamoyl) anthranilic acid, is an anti-allergic agent that inhibits the release of the substances such as histamine and prostaglandins from mast cells and basophils (Koda et al., 1976; Suzawa et al., 1992b). It has been used clinically for the treatment of bronchial asthma, atopic rhinitis and atopic dermatitis. TL has been reported to inhibit the action of transforming growth factor beta (TGF-β), and used clinically for keloids and hypertrophic scar (Suzawa et al., 1992a). Several studies revealed that TL has the beneficial pharmacological effects for various chronic diseases, including hepatic fibrosis (Ikeda et al., 1996; Uno et al., 2008), pulmonary fibrosis (Mori et al., 1991, 1995), and cancer (Izumi et al., 2009; Nie et al., 1997; Noguchi et al., 2003). In spite of these attractive pharmacological effects, TL exhibits the poor dissolution behavior and poor solubility (14.5 μg/ml in water), particularly in acidic condition (0.7 μg/ml in buffer solution of pH 1.2) (The Society of Japanese Pharmacopoeia, 2002), so that the daily dose of TL is relatively high (300 mg/day). This could be a part of reasons for adverse side effects of TL at 300 mg/day in digestive system (Tamai et al., 1999). In addition, because of its chemical structure having a photoreactive cinnamoyl group, TL in the solution state is photochemically unstable, transforming into *cis*-isomer and dimer forms under light exposure (Hori et al., 1999). Thus, the low potency and photostability of TL might limit the clinical use, and these drawbacks need to be improved.

To increase dissolution rate of poorly water-soluble compounds, salt formation (Berge et al., 1977; Serajuddin, 2007) and particle size reduction approaches have been commonly used. Various delivery options, including co-solvents, emulsions (Talegaonkar et al., 2008), and cyclodextrins (Brewster and Loftsson, 2007), were also investigated to improve the dissolution properties of poorly water-soluble drugs. Recently, attention has been drawn to solid dispersion systems, demonstrating the promising results in increasing bioavailability of poorly water-soluble drugs (Onoue et al., 2009), in which the drug is dispersed in solid water-soluble matrices either molecularly or as fine crystalline particles (Chiou and Riegelman, 1971). Several efforts have been made to design highly bioavailable dosage forms for TL by modification of crystalline form or gastroretentive technology (Kawashima et al., 1992,

* Corresponding author. Tel.: +81 54 264 5633; fax: +81 54 264 5635.
E-mail address: onoue@u-shizuoka-ken.ac.jp (S. Onoue).

0928-0987/$ – see front matter © 2009 Elsevier B.V. All rights reserved.
doi:10.1016/j.ejps.2009.12.009